BeBeC-2012-30

A TIME-DOMAIN ANALYSIS OF 3D NON-UNIFORM MOVING ACOUSTIC SOURCES: APPLICATION TO SOURCE IDENTIFICATION AND ABSOLUTE QUANTIFICATION VIA BEAMFORMING

Cédric Camier[a], Jean-François Blais[b], Robby Lapointe[b] and Alain Berry[a]
[a]Université de Sherbrooke
2500 boul de l'université Sherbrooke, Canada, QC J1K2R1
[b]Bombardier Aerospace
P.O. Box 6087, station centre-ville, Montréal , QC, Canada, H3C3G9

ABSTRACT

When applying acoustical imaging techniques of wave fields produced by sources in arbitrary, high-speed motion and sampled by a fixed microphone array, it is necessary to «de-dopplerise » the microphone signals. A careful examination of the related literature reveals a confusion when applying Doppler formulation in term of sound pressure to a monopole source. The aim of this paper is first to carefully detail the analytical and explicit developments of the Doppler effect in term of acoustic pressure for the general case of a density distribution source in a non-uniform and non-rectilinear motion. In the case of arbitrary motion, Lorentz transform is unapplicable and Green's function procedure seems to be the only mathematical tool. An original vectorial closed-form expression of Doppler effect in time-domain has been obtained. The acoustic pressure radiated by a moving monopole has been simulated. Back and forth propagations with other Green functions presented in the literature highlight the impact of the source signal de-dopplerisation on the recovered amplitude. The transfer function introduced in this paper is applied to Delay-And-Sum Beamforming. Although, with respect to the implemented methods, the localisation performances are unchanged. A significant effect on the amplitude is shown and studied with respect to different motion parameters.

1 INTRODUCTION

From an environmental perspective and especially concerning transportation vehicles, localisation and quantification of moving sources are a major study of interest. Helicopter blades noise, turbo-machine noise or more generally high speed railway vehicle sources and aircraft acoustic

sources have to be precisely identified to reduce their annoying effect. One of the problem of analyzing moving sources is the Doppler effect which consists in modulating a source signal in both frequency and amplitude.

By analysing the wave field sampled by a microphone array via acoustical image techniques, microphone signals need to be "de-dopplerised" when applying Delay-And-Sum algorithms or more evolved ones. In several works, only the frequency shift of Doppler effect is considered. For example, Siller has identified the noise source contributions on a fly-over aircraft by the help of de-dopplerised spectra and Beamforming [12], as well as Zechel [14] in time-domain. Applying an inverse source density model, Zillman [15] uses the same assumption. Others works consider amplitude modulation by keeping a source speed dependence in the microphone signal correction. Sijtsma and Oerlemans [6–8, 11] use a time-domain and vectorial formulation or a frequency formulation with the assumptions of uniform and rectilinear movement. Generally, this last assumption is widespread because of the simplicity of the formulation in term of angle between the trajectory direction and the sound emission direction toward the microphone. By this way, Searle [10] has described analytically the delay between the emission time and the reception time whereas Valiere and Poisson [9, 13] have used different time-frequency transforms applied to Beamforming dedicated to high speed sources.

One can find in [5] and in [4] the complete formulation of Doppler effect in the unidirectional case and uniform movement developed by employing a Lorentz transformation. The case of a harmonic monopole source is also considered in sub- and supersonic movements. In the present paper, emphasis is notably put on the source quantity involved in the mentioned developments. Indeed, a confusion could raise when applying Doppler formulation in term of pressure to a monopole source strength. In the case of non-uniform and non-rectilinear motion, Lorentz transform is inapplicable. Green's function procedure seems to be the only mathematical tool [2, 3].

The outlines of this paper is first to carefully detail the analytical and explicit developments of Doppler effect in term of acoustic pressure for the general case of density distribution source in arbitrary motion. Then, results are compared to uniform rectilinear motion development based on Lorentz transform. Then, the two terms of the Doppler effect written in terms of pressure are numerically compared. The formulation is then applied to the Delay-And Sum Beamforming algorithm. The error made by considering other kind of de-dopplerisation algorithms presented in the literature are then highlighted and quantified with the help of a back and forth propagation between an emitting source and a observation point. Cumulated errors are also emphasised with Beamforming map simulation results.

2 WAVE FIELD GENERATED BY A POINT SOURCE IN ARBITRARY MOTION

When the source motion is not rectilinear and uniform, the Lorentz transform can not be applied because the source referential is not galilean anymore. In order to develop the potential wave field and consequently the pressure wave field due to a moving acoustic source, we use the Green formulation by starting with the wave equation written for the acoustic velocity potential. Following developments are inspired from [3] which solves the Doppler problem in the general case of a wave equation including a wave function excitation. Applied to the acoustic domain, the wave function involved in the particular formulation specifically denotes a speed potential

source and not a pressure source. This last distinction is important because in the case of moving sources, the resulting time-pressure trace differs by confusing the two quantities. This will be extensively detailed in the sequel.

The acoustic and medium quantities given in Table 1 are considered. In particular, the acoustic velocity potential is noted $\Psi(\mathbf{r},t)$.

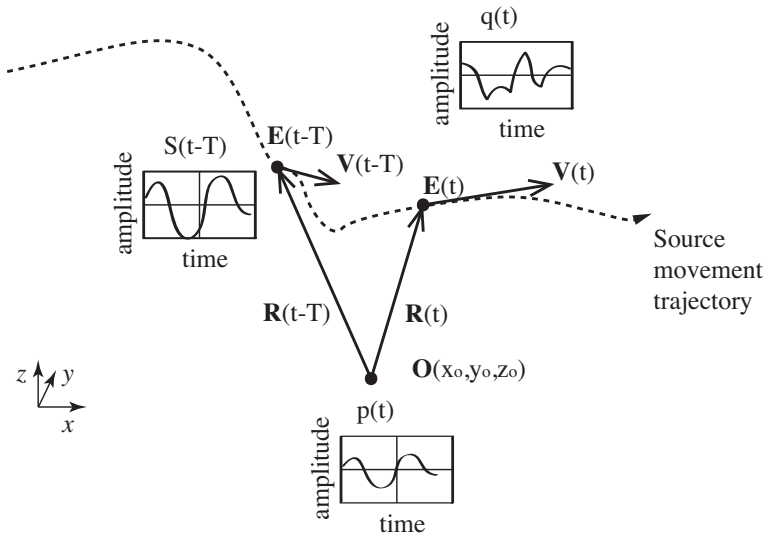

Figure 1: Geometry of the source moving with an arbitrary motion with respect to a fixed observation point.

In Fig. 1, one considers a punctual acoustic source $q(t)$ moving in an arbitrary trajectory $\{\mathbf{E}(t)\}_{t\in\mathrm{R}}$ at speed $\mathbf{V}(t)$. The observation point is localized at $\mathbf{O}(x_o,y_o,z_o)$ and receives the acoustic pressure $p(t)$. First, the source strength density of a punctual source localised at $\mathbf{E}(t)$ writes:

$$Q(\mathbf{r},t) = \frac{\mathbf{1}}{\rho} q(t)\delta(\mathbf{r}-\mathbf{E}(t)). \tag{1}$$

The wave equation written in terms of velocity potential is expressed by:

$$\Delta\Psi - \frac{1}{c^2}\frac{\partial^2\Psi}{\partial t^2} = -Q(\mathbf{r},t), \tag{2}$$

and the pressure derived from the acoustic velocty potential is given by:

$$p = -\rho\frac{\partial\Psi}{\partial t}. \tag{3}$$

MEDIUM PROPERTIES	
ρ	Volume density of mass
c	Acoustic wave celerity
GEOMETRICAL QUANTITIES	
$\mathbf{E}$	Source trajectory
$\mathbf{r}$	Cartesian co-ordinates
t	time in the fixed observation point referential
ACOUSTIC WAVE FIELD QUANTITIES	
$p(\mathbf{r},t)$	aAoustic pressure
$\Psi(\mathbf{r},t)$	Acoustic velocity potential
$G(\mathbf{r},t)$	Green function
ACOUSTIC SOURCE QUANTITIES	
$Q(\mathbf{r},t)$	Source-distribution density [kg/m^3]
$q(t)$	Source-distribution density time component

Table 1: Physical and material properties of the carrying medium and geometrical quantity nomenclature

2.1 Velocity potential solution

The Green function G associated to the differential equation

$$\Delta G - \frac{1}{c^2}\frac{\partial^2 G}{\partial t^2} = -\delta(\mathbf{r}-\mathbf{r}',t) \tag{4}$$

is the causal solution:

$$G(\mathbf{r},\mathbf{r}',t) = \frac{\delta\left(t-t'-\dfrac{|\mathbf{r}-\mathbf{r}'|}{c}\right)}{4\pi|\mathbf{r}-\mathbf{r}'|} \tag{5}$$

and the pertaining source-type representation, which is here the potential velocity, is given by the time-convolution :

$$\Psi(\mathbf{r},t) = \int_0^\infty \iiint_{V\subset x'} G(\mathbf{r},\mathbf{r}',t)Q(\mathbf{r}',t-t')dV(\mathbf{r}')dt' \tag{6}$$

with x' the spatial support of the source.

Then, for a punctual acoustic source localized by $\mathbf{E}$, described by Eq. (1):

$$\begin{aligned}\Psi(\mathbf{r},t) &= \int_0^\infty G(\mathbf{r},\mathbf{E}(t-t'),t')q(t-t')dt' \\ &= \tfrac{1}{\rho}\int_0^\infty \frac{\delta\left(t-\dfrac{|\mathbf{r}-\mathbf{E}(t-t')|}{c}\right)}{4\pi|\mathbf{r}-\mathbf{E}(t-t')|}q(t-t')dt'.\end{aligned} \tag{7}$$

One introduces the coordinates change:

$$\begin{cases} \tau = t' - \dfrac{|\mathbf{r}-\mathbf{E}(t-t')|}{c}, \\ \dfrac{\partial \tau}{\partial t'} = 1 - \dfrac{\mathbf{V}(t-t')\cdot(\mathbf{r}-\mathbf{E}(t-t'))}{c|\mathbf{r}-\mathbf{E}(t-t')|} \end{cases} \tag{8}$$

t' could also be written as a function of τ, under conditions described in [2]. By introducing the function T,

$$t' = T(\mathbf{r},t,\tau), \tag{9}$$

Eq. (7) can then be reduced to:

$$\Psi(\mathbf{r},t) = \frac{\mathbf{1}}{\rho}\int_{\tau_{min}}^{\infty} \frac{\delta(\tau)}{4\pi|\mathbf{r}-\mathbf{E}(t-T(\mathbf{r},t,\tau))|} q(t-T(\mathbf{r},t,\tau))\frac{dt'}{d\tau}d\tau, \tag{10}$$

then, the time derivation of t' gives:

$$\Psi(\mathbf{r},t) = \frac{\mathbf{1}}{\rho}\int_{\tau_{min}}^{\infty} \frac{\delta(\tau)q(t-T)}{4\pi|\mathbf{r}-\mathbf{E}(t-T)|\left(1-\dfrac{\mathbf{V}(t-T)\cdot(\mathbf{r}-\mathbf{E}(t-T))}{c|\mathbf{r}-\mathbf{E}(t-T)|}\right)}d\tau. \tag{11}$$

in which

$$\tau_{min} = -\frac{|\mathbf{r}-\mathbf{E}(t)|}{c} \leq 0. \tag{12}$$

According to Eq. (8), the time $T(\mathbf{r},t,0)$ is the delay of the wave propagation from the emission point at time $t-t'$ to the observation point. The distance at time $t-t'$ where noted $R^+ = R^+(t) = R(t-T)$. $\mathbf{R}^+(t) = \mathbf{E}(t-T) - \mathbf{O}$ denotes the corresponding vector. By using the convolution property of the Dirac function and evaluated at $\mathbf{O}(x_o,y_o,z_o)$,the potential velocity is expressed by:

$$\Psi(\mathbf{O},t) = \frac{q(t-R^+/c)}{4\pi\left(R^+(t) - \frac{1}{c}\mathbf{V}(t-R^+/c))\cdot\mathbf{R}^+(t)\right)}, \tag{13}$$

where $q(t)$ is the source signature and, more precisely in this description, the amplitude of the acoustic mass density $Q(t)$. One remembers that this quantity comes from the wave equation expressed in terms of pressure with only a volume debit acoustic source and no acoustic force in the right handside of Eq. (2).

2.2 Pressure solution

Relatively to Eq. (3) temporal derivation of Eq. (13) writes

$$p(\mathbf{O},t) = -\frac{q'(t-R^+(t)/c)\dfrac{\partial}{\partial t}\left(t-\dfrac{R^+}{c}\right)}{4\pi\left(R^+(t)-\dfrac{1}{c}\mathbf{V}(t-R^+(t)/c)\cdot\mathbf{R}^+(t)\right)} + \frac{q(t-R^+(t)/c)\dfrac{\partial}{\partial t}\left(R^+(t)-\dfrac{1}{c}\mathbf{V}(t-R^+(t)/c)\cdot\mathbf{R}^+(\mathbf{t})\right)}{4\pi\left(R^+(t)-\dfrac{1}{c}\mathbf{V}(t-R^+(t)/c)\cdot\mathbf{R}^+(t)\right)^2}. \tag{14}$$

The time differentiation of the delayed distance R^+ between source and observation point needs to be explicitly developed. The temporal derivation of R^+ could be expressed with the help of the distance vector $\mathbf{R}^+(t)$ and the speed vector $\mathbf{V}$:

$$\frac{\partial R^+(t)}{\partial t} = -\frac{\mathbf{V}(t-R^+(t)/c)\cdot\mathbf{R}^+(\mathbf{t})}{R^+}\cdot\frac{\partial}{\partial t}\left(t-\frac{R^+(t)}{c}\right). \tag{15}$$

When factorizing $\dfrac{\partial R^+(t)}{\partial t}$, one obtains :

$$\frac{1}{c}\frac{\partial R^+(t)}{\partial t} = -\frac{\mathbf{M}(t-R^+(t)/c)\cdot\mathbf{R}^+(t)}{R^+-\mathbf{M}(t-R^+(t)/c)\cdot\mathbf{R}^+(t)} \tag{16}$$

where

$$\mathbf{M} = \mathbf{V}/c$$

. Similar developments are performed for the useful vectorial quantities

$$\frac{\partial \mathbf{R}^+(t)}{\partial t} = \mathbf{V}(t-R^+(t)/c)\cdot\frac{R^+(t)}{R^+-\mathbf{M}(t-R^+(t)/c)\cdot\mathbf{R}^+(t)} \tag{17}$$

and

$$\frac{\partial \mathbf{V}(t-R^+/c)}{\partial t} = \mathbf{A}(t-R^+(t)/c)\cdot\frac{R^+(t)}{R^+-\mathbf{M}(t-R^+(t)/c)\cdot\mathbf{R}^+(t)}, \tag{18}$$

where $\mathbf{A}(t)$ is the acceleration of the source at time t. Finally, the pressure signal due to an acoustic source in arbitrary motion could then be fully developed from Eq. (14)

$$p(\mathbf{O},t) = \underbrace{\frac{q'\big(t-R^+(t)/c\big)R^+(t)}{4\pi\left(R^+(t)-\frac{1}{c}\mathbf{V}(t-\mathbf{R}^+(t)/c)\cdot\mathbf{R}^+(t)\right)^2}}_{q_1} + \underbrace{\frac{q(t-R^+(t)/c)\cdot R^+(t)}{4\pi\left(R^+(t)-\frac{1}{c}\mathbf{V}\cdot\mathbf{R}^+(t)\right)^3}\cdot\left(\frac{\mathbf{V}^+\cdot\mathbf{R}^+(t)}{R^+(t)}+\frac{\mathbf{A}^+\cdot\mathbf{R}^+(t)}{c}-\frac{V^{+2}}{c}\right)}_{q_2}. \tag{19}$$

To save some place, some arguments are squeezed by introducing the quantities $V^+ = V(t-R^+/c)$, $\mathbf{V}^+ = \mathbf{V}(t-R^+/c)$ and $\mathbf{A}^+ = \mathbf{A}(t-R^+(t)/c)$.

This original formulation expresses the acoustic pressure in an observation point and generated by a radiating acoustic monopole parametrised by source-distribution density time component $q(t)$, position, velocity vector and acceleration vector, respectively noted $\mathbf{R}(t)$, $\mathbf{V}(t)$, $\mathbf{A}(t)$ in the time referential of the observation point. This formulation extends the classical case of the uniform-speed motion Doppler effect. By applying this formulation to a uniform-speed motion, this expression becomes identical to the Ingard and Morse result given in [5] which is recalled here:

$$p(\mathbf{r},t) = \frac{1}{4\pi}\frac{q'(t-R^+(t)/c)}{R^+(t)\cdot(1-M\cos(\theta))^2} + \frac{V(\cos(\theta)-M)}{4\pi R^+(t)^2(1-M\cos(\theta))^3}q(t-R^+(t)/c), \tag{20}$$

with

$$R^+(t) = \frac{V\cdot(x_0-Vt)+\sqrt{(x_0-Vt)^2+(y_0^2+z_0^2)(1-M^2)}}{(1-M)^2} \tag{21}$$

and for the geometry problem and notations described in Fig. 2.

2.3 Simulations

In order to evaluate the influence of the q_1 and q_2 terms of Eq. (19), simulations of acoustic pressure evaluated at a fixed point and emitted by a rectilinear and uniform moving source have been made. Simulation results are shown in Fig. 3.

Fig. 3(a),(b) and (c) show the contribution of the first term q_1 and the second term q_2 of Eq. (19), for a range of altitude, frequency and velocity. Generally speaking, the contribution of the term q_2 is very small (inferior to q_1 by approximately 70 dB), compared to the first one. One notes the cancellation of q_2 when $cos(\theta) = M$ in Eq. (20). Fig. 3(a) shows that the closer is the source trajectory to the observer location, the larger is the amplitude impact of the Doppler effect. Fig. 3(b) shows that the contribution of q_2 raises when the frequency of the source diminishes. Indeed, the simulation keep constant the mean square source pressure amplitude, so the amplitude of $\frac{\partial Q}{\partial t}$ introduced in Eqs (2) and (3). For harmonic signals, q amplitude differs

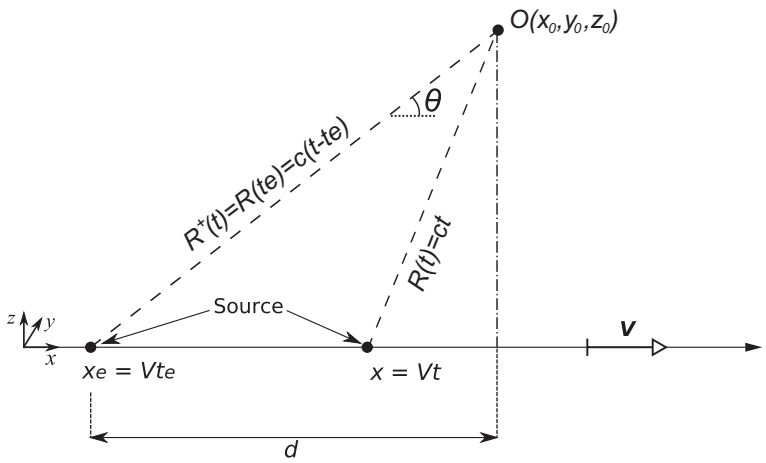

Figure 2: Geometry of the source moving rectilinearly and with a constant speed vector $\mathbf{V}$ *with respect to a fixed observation point localised at* $O(x_o, y_o, z_o)$*. The norm of* $\mathbf{V}$ *is noted* V*. xs and xe are the position of the moving source at time* t *and* te *respectively.* $R(t)$ *is the distance between observation point and moving source at time* t*. The mach number is M=V/c.*

from q' amplitude by the factor $1/(2 * \pi * f)$, which is consistent with the difference observed in the depicted q_2 curves of Fig. 3(b). Fig. 3(c), one observes that both q_1 and q_2 show an asymptotic value weaker when the source goes away than when the source approaches. This is due to the compression of the waves when the sources approaches and on the opposite, the depression of the wave when it moves away.

Considering typical altitude and trajectory of aircraft during flyover measurements, as well as the frequency content of the noise source, we consider in the sequel that the term q_2 is negligible in the Doppler effect compensation.

3 APPLICATION TO BEAMFORMING

In the context of vehicle acoustic sources identification, Doppler effect is often a major effect to correct when applying localization algorithms on microphone array recordings. The theoretical previous developments are applied to a widely used identification algorithm firstly introduced in 1977: the Delay-and-Sum [1], called later Beamforming. The first next section reports simulation results, in order to validate and analyse the formulation proposed in Eq. (19). The classical equation of Beamforming is recalled in the time-domain. The principle idea consists in delaying and summing the measured pressures $p_i(t)$ of a microphone array to enhance the signal emanating from a focal position. The time-delay is chosen to be the spherical radiation's one in the following computations (the Beamforming algorithm used is well-known as "Focused Delay-and-Sum"). Considering a focus point $\mathbf{r}$ at distances R_i of each microphone i of the

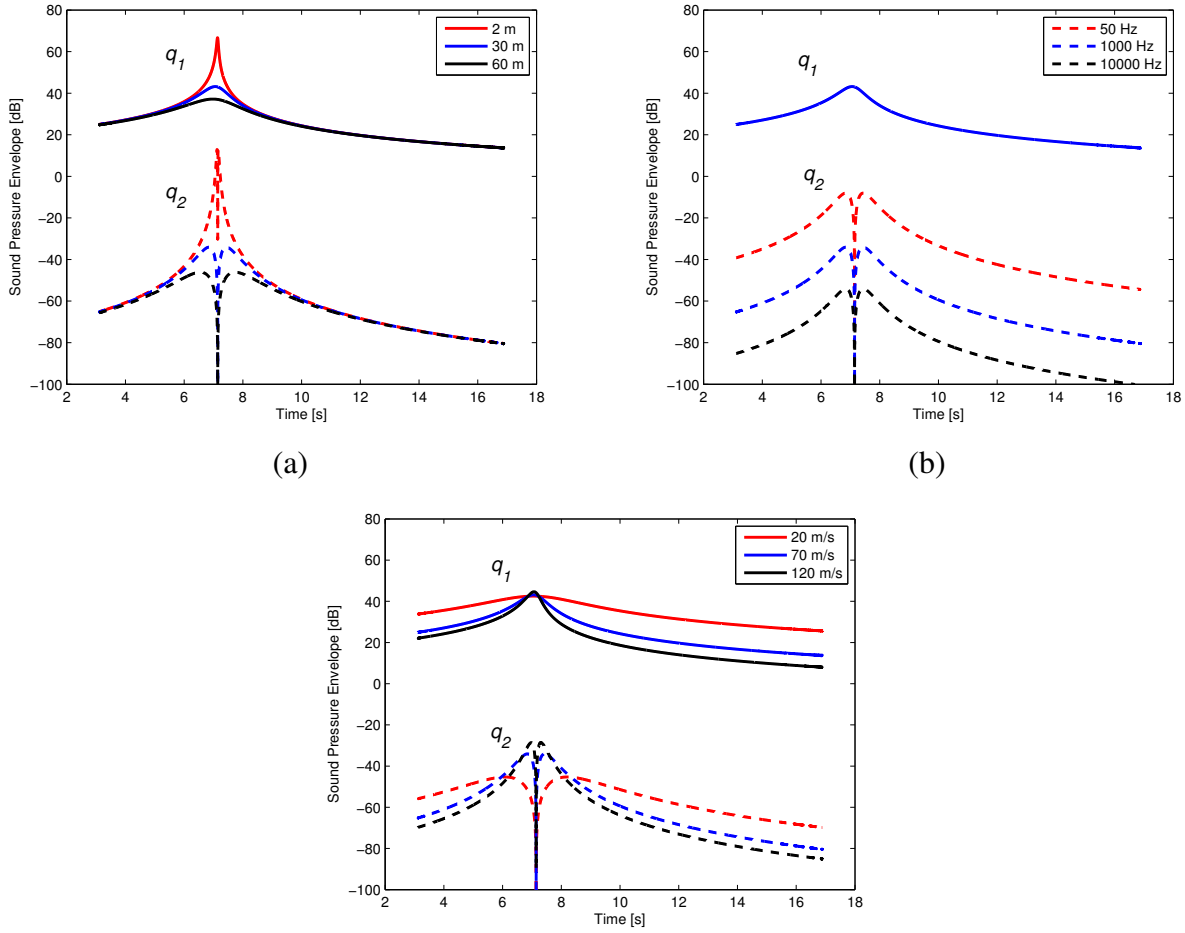

Figure 3: Comparison of the contribution of term q_1 and q_2 of Eq. 19 in a rectilinear uniform motion with respect to (a) the altitude of the trajectory , (b) the source frequency and (c) the motion speed. When a parameter has no mentioned variation, it refers to the typical case : $[z, f, V]$=[30 m , 1000 Hz, 70 m.s^{-1}].

N-microphone-array, the output $B(\mathbf{r})$ of Beamforming is given by

$$B(t,\mathbf{r}) = \frac{1}{N}\sum_{i=1}^{N} R_i p_i(t-\Delta_{\mathbf{r}i})$$

where

$$\Delta_{\mathbf{r}n} = \frac{\mathbf{r}-R_i(\mathbf{r})}{c}.$$

In order to perform the temporal Delay-And-Sum with de-dopplerised pressure signals, we use the pressure formulation of Doppler effect Eq. (19). It has been shown that the term q_2 of the equation can be neglected. It is consequently omitted in the following developments. Moreover,

in order to sum de-dopplerised signals in the time-referential of the moving source, the changes of coordinate

$$t'' = t + R_i^+(t)/c$$

are considered. The implemented Beamforming finally writes:

$$\underbrace{B\big(t,\mathbf{r}(t)\big) = \sum_{i=1}^{N} \frac{4\pi\left(R_i(t) - \frac{1}{c}\mathbf{V}(t)\cdot\mathbf{R}_i(t)\right)^2}{R_i(t)} p\big(R_i(t), t + R_i(t)/c\big)}_{\text{DAS 1}} \tag{22}$$

where $\mathbf{R}_i(t)$ is the distance vector between the moving source and the i^{th} microphone. This de-dopplerisation method is noted DAS 1 (Delay-And-Sum) in the sequel.

In order to evaluate the error made by applying a different de-dopplerisation method, the two next Beamforming algorithms are considered :

$$\underbrace{B\big(t,\mathbf{r}(t)\big) = \sum_{i=1}^{N} 4\pi\left(R_i(t) - \frac{1}{c}\mathbf{V}(t)\cdot\mathbf{R}_i(t)\right) p\big(R_i(t), t + R_i(t)/c\big)}_{\text{DAS 2}} \tag{23}$$

which will be noted DAS 2, and

$$\underbrace{B\big(t,\mathbf{r}(t)\big) = \sum_{i=1}^{N} 4\pi R_i(t)\, p\big(R_i(t), t + R_i(t)/c\big)}_{\text{DAS 3}} \tag{24}$$

noted as DAS 3. These methods and in particular the DAS 2 one are especially tested and studied in this paper because they have been used regularly in the localisation literature. The authors want to emphasis the error eventually made by applying the misleading de-dopplerisation method to the pressure source signal considered.

3.1 Retro-propagation simulations

In order to both validate the DAS 1 method and quantify the error that may be induced by DAS 2 and DAS 3, a reception pressure signal produced at one observation point by a moving emitting source is retro-propagated to the exact location of the moving source by the three introduced methods (by setting N=1 in Eqs. (22),(23) and (24)).

The propagation from the moving source to the reception is made with Ingard and Morse formulation Eq. (20), as it is chosen as the reference equation. The simulation involves a 1 Pa_{RMS} harmonic monopole moving in a rectilinear and uniform speed equal to 70 $m.s^{-1}$ on a 30-meter altitude trajectory. The trajectory of the moving source crosses the exact zenith of the observation point at t =10 s. Results of the three kinds of retro-propagation computations are given in Fig. 4. When the retro-propagation is computed with DAS 1, the original source signal is exactly recovered and the SPL is equal to 94 dB. When applying DAS 2 and DAS 3, the absolute error reach 2 dB and 4 dB respectively when the source approaches the observation point location. This absolute error is weaker in the moving away motion. Figure 4(a) shows the en-

velope of the recovering source signal computed with the L_{fast} method. Figure 4(b) shows the polar diagram of the Sound Pressure Level (SPL) with respect to the emission angle, 0° being the front of the source and 180° being the front of the source with respect to its motion. The polar diagram represents the error which can be made by evaluating the directivity of the source along a trajectory via DAS 2 or DAS 3.

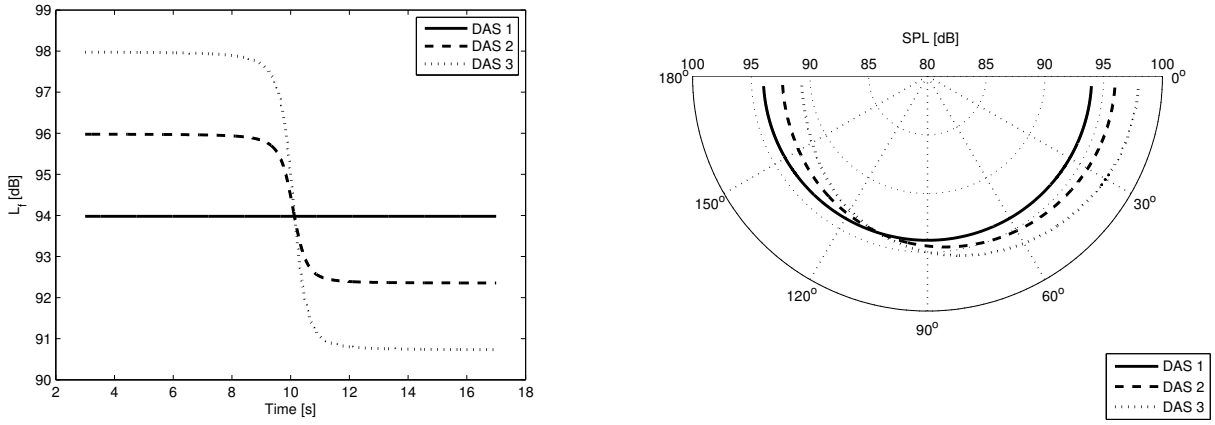

(a) (b)

Figure 4: (a) SPL with respect to time and (b) SPL with respect to the approach angle of the retro-propagated observation pressure signal computed with DAS 1*,* DAS 2 *and* DAS 3 *compared to the original source signal. The source is defined by its mean square pressure amplitude, frequency, altitude and speed being equal to 1 Pa_{RMS}, 1000 Hz, 30 m and 70 m.s^{-1} respectively.*

In particular, the error due to DAS 2 de-dopplerisation on the SPL estimation and on the resulted directivity pattern is quantified for both an altitude range and a speed range . The source signal mean square pressure amplitude is chosen to be 1 Pa_{RMS} and its frequency to be 1000 Hz. Fig. 5(a) and (b) show the SPL of the retro-propagated observation pressure signal computed with DAS 2 for an altitude range equal to [1 70] m and for a constant speed equal to 70 m.s^{-1}. The asymptotic errors are constant and approximately equal to 2 dB and -1.7 dB for the approaching motion and moving away motion respectively. The transition between both error is shaper when the trajectory is closer to the source location. Fig. 5(c) and (d) show the SPL of the retro-propagated observation pressure signal computed with DAS 2 for an speed range equal to [1 100] m.s^{-1} and for a constant altitude equal to 30 m. The error between the retro-propagation and the reference increases with the speed amplitude and reaches 3 dB for the approaching 100 m.s^{-1} speed motion. For each case, the exact correspondence of the reference source signal and the signal computed with DAS 1 retro-propagation have been verified.

3.2 Beamforming map simulations

A virtual 80-microphone array, which corresponds to the home-build microphone array of GAUS laboratory, is considered. The array geometry considers a double layer (12.25 cm vertically spaced) rectangular array and aligned on a horizontal grid with spacing of 12.25 cm. The

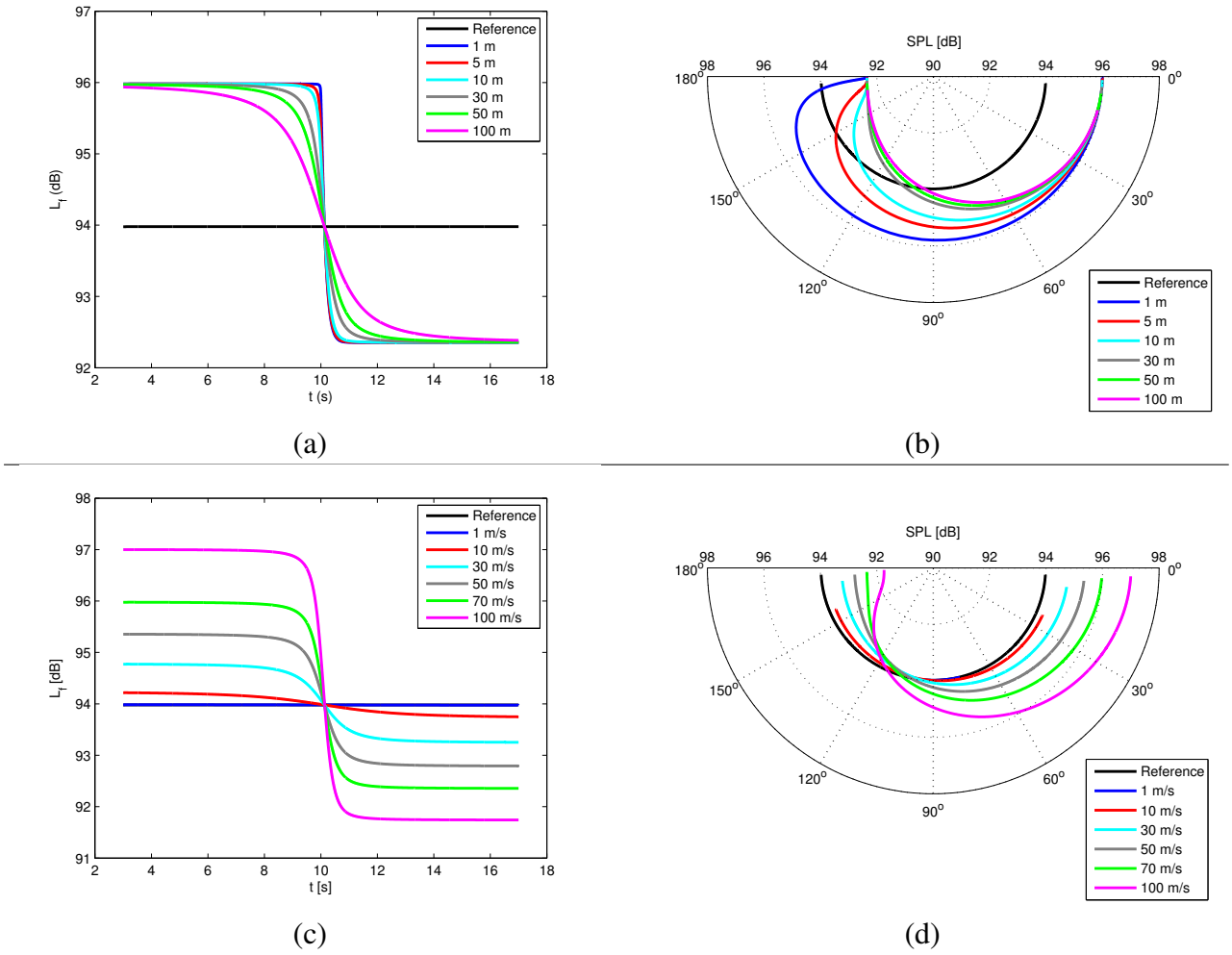

Figure 5: (a) SPL with respect to time and (b) SPL with respect to the approach angle of the retro-propagated observation pressure signal computed with DAS 2 *for the depicted altitude range and with speed being equal to 70 m.s^{-1}. (c) SPL with respect to time and (d) SPL with respect to the approach angle of the retro-propagated observation pressure signal computed with* DAS 2 *for the depicted speed range and with altitude being equal to 30 m.*

array width, length and height are equal to 0.993 m, 1.3475 m and 12.25 cm, respectively.

An example of localisation with Doppler effect compensation by DAS 1 and DAS 2 is given in Fig. 6. The simulations implies a harmonic monopole in rectilinear and uniform motion at speed 100 m.s^{-1}, travelling at an altitude equal to 1.3 m above the array. Its frequency is fixed to 1000 Hz and the mean square pressure amplitude is chosen to be 1 Pa$_{RMS}$. A 13×13 point mapping is computed around the 1.3-meter altitude zenith of the array center. This mapping is a $2m \times 2m$ square synchronised with the source motion. The sampling frequency is equal to 48000 Hz and the time-window used for the localisation algorithms is 500 temporal points. Different initial positions are considered, referring to approaching, zenith-close and moving

away motion types. The problem geometry is exemplified in Fig 6 for the zenith-close motion type case.

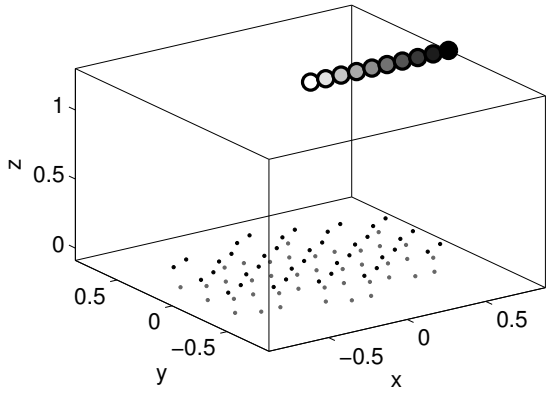

Figure 6: Geometry of the Beamforming map simulations for the zenith type motion case. The array geometry is plotted as little black and grey dots corresponding to its upper and lower layer respectively. The source motion is under-sampled to 10 points containing the initial and the final position of the time-window used in algorithm computations. The initial position is plotted by a white-filled big dots and the later positions are filled with a grey scale.

As expected by the observation of the delay compensation inside the time-dependency of the pressure term in Eqs. (22),(23) , the localisation is exactly the same for the both algorithms. Nevertheless, a significant difference is made in the quantification of the absolute value. Table 2 gives the precise maximum amplitudes of Beamforming maps. One notes a cumulated over-estimation of the source amplitude of 1 dB for the approaching motion type and a cumulated under-estimation of approximately 1.5 dB for the moving away motion type.

The speed and geometry parameters have been chosen to highlight the effect of the de-dopplerised algorithm used. The presented results concern a high speed motion detection. For the cases of exterior slower motion identification, the Doppler effect amplitude correction is thus a less important parameter with regard to the effect of some experimental or numerical parameters as the effect of the wind or the sampling frequency. Nevertheless, as the evolution of absolute quantification algorithms will inexorably compensate the imprecision of each parameters included in current or future algorithms, this study is expected to clarify a confusion observed in literature when taking into account the Doppler effect, from which the contribution could be non-negligible in some cases and so has to be carefully applied.

4 CONCLUSION

A complete analytical and vectorial formula of the 3D arbitrary motion Doppler effect in term of pressure have been developed and compared to the uniform rectilinear motion case established by Ingard and Morse. Nevertheless, the evaluation for different kinds of motion proves that the

Motion type	DAS 1		DAS 2	
	max(q')	max(SPL)	$\max_{RMS}(B/(4\pi))$	max(SPL)
Approaching motion type	.9998 Pa.m	93.98 dB	1.1185 Pa.m	94.95 dB
Zenith-close motion type	1.0005 Pa.m	93.98 dB	.9331 Pa.m	93.38 dB
Moving away motion type	1.0055 Pa.m	94.03 dB	0.8205 Pa.m	92.26 dB
Variation maximum along the motion	0.0057 pa.m	**0.05 dB**	0.29 8pa.m	**2.69 dB**

Table 2: Maximum amplitudes of Beamforming maps shown in 7.

second term q_2 originally developed is negligible. The study of different de-dopplerisation algorithms presented in the literature have been studied and quantified by the help of back and forth propagation computations of a moving source pressure signal. Errors made have been shown in term of absolute quantification, evolution of the instantaneous amplitude of the recovered source signal and estimation of the directivity pattern. The misleading de-dopplerisation methods have been also evaluated on Beamforming maps and show significant cumulative errors for the high-speed motion depicted.

5 AKNOWLEDGMENTS

Adrianus T. de Hoop is warmly thanked for the very profitable correspondence we conducted about his previous developments. This work has been supported by the NSERC Industrial Research Chair in Aviation Acoustics and the Green Aviation Research & Development Network (GARDN).

References

[1] J. Billingsley and R. Kinns. "The acoustic telescope." *J. Sound Vib.*, 51, 23–54, 1977.

[2] A. T. de Hoop. "Fields and waves excited by impulsive point sources in motion - the general 3d time-domain doppler effect." *Wave motion*, 43, 116122, 2005.

[3] A. T. de Hoop. "Electromagnetic radiation from moving, pulsed source distributions: The 3d time-domain relativistic doppler effect." *Wave motion*, 46, 74–77, 2009.

[4] M. E. Goldstein. *Aeroacoustics*. Mc Graw-Hill International book Company, 1976.

[5] P. M. Morse and K. U. Ingard. *Theoretical Acoustics:*. Princeton University Press, 1987.

[6] S. Oerlemans. *Detection of aeroacoustic sound sources on aircraft and wind turbines*. Ph.D. thesis, Universiteit Twente, 2009.

[7] S. Oerlemans and P. Sijtsma. "Determination of absolute levels from phased array measurements using spatial source coherence." Technical report, National Aerospace Laboratory NLR, 2002.

[8] S. Oerlemans and P. Sijtsma. "Acoustic array measurements of a 1: 10: 6 scaled airbus a340 model." Technical report, National Aerospace Laboratory NLR, 2004.

[9] F. Poisson, J.-C. Valiere, and P. Herzog. "High speed sound sources localization using bilinear time-frequency transformation." *J. Applied Acoustics*, 53(1-3), 1–13, 1998.

[10] S. J. Searle. "Efficient matched processing for localisation of moving acoustic source." *Signal Processing*, 85, 1787–1804, 2005.

[11] P. Sijtsma and R. Stoker. "Determination of absolute contributions of aircraft noise components using fly-over array measurements." Technical report, National Aerospace Laboratory NLR, 2004.

[12] H. Siller, M. Drescher, G. Saueressig, and R. Lange. "Fly-over source localisation on a boeing 747-400." In *Berlin Beamforming Conference*. 2010.

[13] J.-C. Valiere, F. Poisson, C. Depollier, and L. Simon. "High-speed moving source analysis using chirplet." *IEEE Signal Procesing Letters*, 6(5), 1999.

[14] G. Zechel, A. Zeibig, and M. Beitelschmidt. "Tine-domain beamforming on moving objects with known trajectories." In *Berlin Beamforming Conference*. 2010.

[15] J. Zillmann and C. Cariou. "Array analysis aircraft fly-over measurements." In *Berlin Beamforming Conference*. 2010.

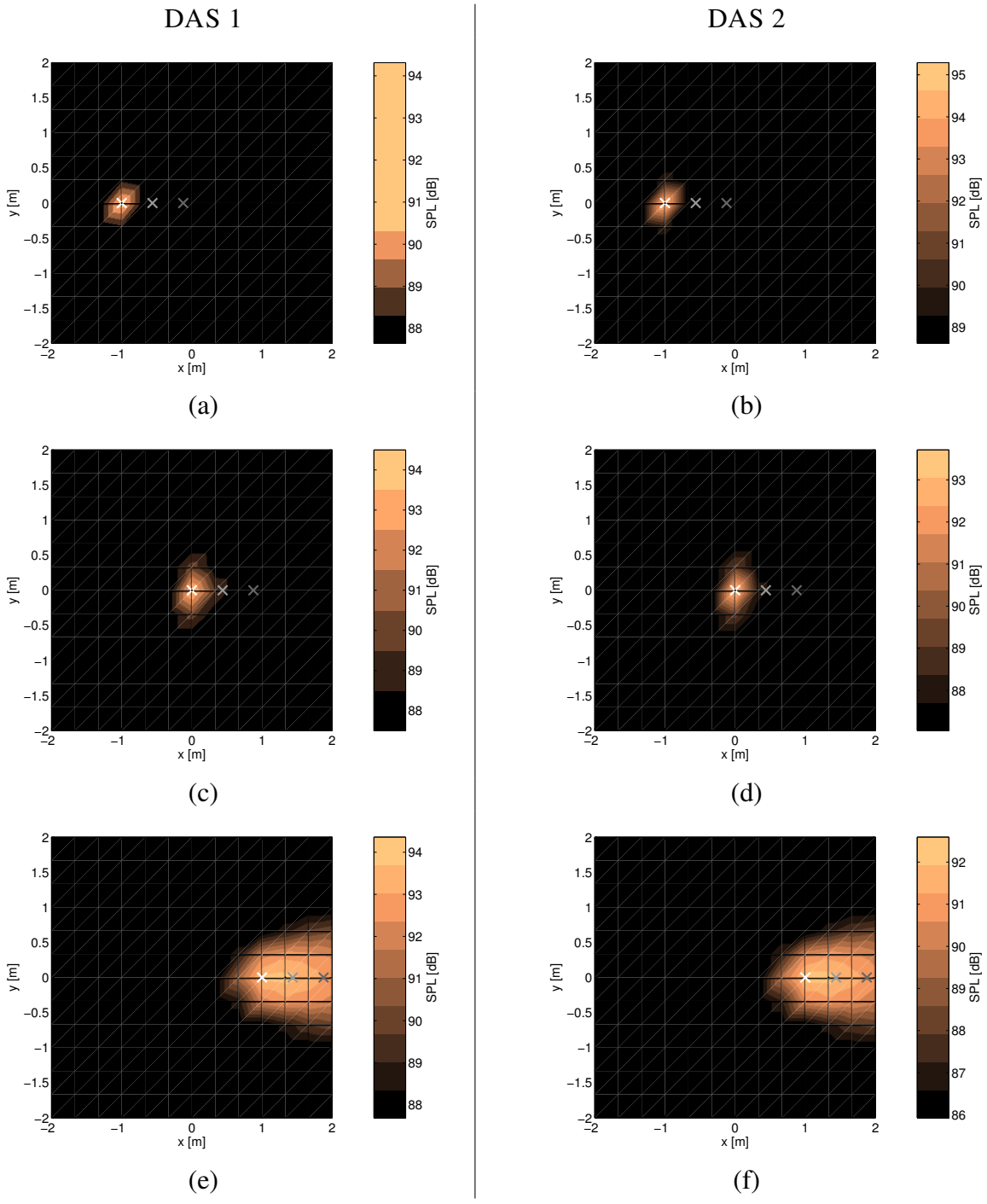

Figure 7: Comparison of Beamforming maps computed from a moving source with both DAS 1 *and* DAS 2. *White crosses indicate the initial positions of the source and where the de-dopplerisation methods are computed. Grey and dark-grey crosses indicates respectively the mean position and the final position along the time window chosen in the computation. Approaching, zenith-close and moving away motion type referred to the array center are considered to highlight the under- or over-estimation effect of the* DAS 2. *Complementary to this figure, Table 2 gives the precise maximum amplitudes of Beamforming maps.*